



Oxygen reduction reaction mechanism on nitrogen-doped graphene: A density functional theory study

Liang Yu ^{a,1}, Xiulian Pan ^{a,1}, Xiaoming Cao ^{b,2}, P. Hu ^{b,*}, Xinhe Bao ^{a,*}

^a State Key Laboratory of Catalysis, Dalian Institute of Chemical Physics, The Chinese Academy of Sciences, Dalian 116023, China

^b School of Chemistry and Chemical Engineering, The Queen's University of Belfast, Belfast BT95AG, United Kingdom

ARTICLE INFO

Article history:

Received 29 March 2011

Revised 12 June 2011

Accepted 13 June 2011

Available online 16 July 2011

Keywords:

Oxygen reduction reaction mechanism

Nitrogen-doped graphene

Density functional theory

Catalysis

Reaction kinetics

ABSTRACT

Nitrogen-doped graphene (N-graphene) was reported to exhibit a good activity experimentally as an electrocatalyst of oxygen reduction reaction (ORR) on the cathode of fuel cells under the condition of electropotential of ~0.04 V (vs. NHE) and pH of 14. This material is promising to replace or partially replace the conventionally used Pt. In order to understand the experimental results, ORR catalyzed by N-graphene is studied using density functional theory (DFT) calculations under experimental conditions taking the solvent, surface adsorbates, and coverages into consideration. Two mechanisms, i.e., dissociative and associative mechanisms, over different N-doping configurations are investigated. The results show that N-graphene surface is covered by O with 1/6 monolayer, which is used for reactions in this work. The transition state of each elementary step was identified using four different approaches, which give rise to a similar chemistry. A full energy profile including all the reaction barriers shows that the associative mechanism is more energetically favored than the dissociative one and the removal of O species from the surface is the rate-determining step.

© 2011 Elsevier Inc. All rights reserved.

1. Introduction

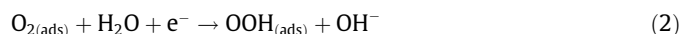
Wide efforts are being made to replace or reduce the usage of precious Pt catalyst as the cathode of fuel cells. Nitrogen-doped carbon materials exhibit promising potentials for taking this role [1–9]. In cyclic voltammetry measurements, N-graphene showed oxygen reduction reaction (ORR) activity that is comparable to Pt/C catalyst in alkaline solution [10]. Among the two most stable types of doped N, i.e., pyridinic and graphitic N [11], X-ray absorption spectroscopy (XAS) analyses suggested that catalysts with a relatively larger amount of graphitic N exhibit higher ORR activity than those with a relatively larger amount of pyridinic N [7], as also indicated in a theoretical calculation [17]. However, the ORR mechanism catalyzed by the N-graphene remains elusive. In this work, we carried out DFT calculations to investigate the reaction mechanism in particular the kinetics in this process under reaction conditions.

Earlier studies have shown that O₂ can be reduced following two different paths. One is the so-called “4e⁻ reduction” in which O₂ is completely reduced to two OH⁻ and this is the predominant

path [10,12]. The other is called “2e⁻ reduction” in which O₂ is partially reduced to OOH⁻. The second path leads to inadequate use of O₂ and gives rise to a lower potential than the first path. Several DFT studies suggested that the ORR activity on metal surfaces is limited by two rate-determining steps: formation of OOH_(ads) and removal of OH_(ads) [13,14]. However, facilitating one step will hinder the other one because the binding strengths of OOH_(ads) and OH_(ads) are directly correlated to each other and also to that of O_(ads) [13,14]. It was proposed that the ORR activity on different metals can be described as a function of the adsorption energy of O_(ads), which yields a volcano curve. Pt sits very close to the peak of the volcanic curve, indicating that Pt is the best catalyst for the ORR [15]. This was considered to be a simple way to predict ORR activity of new materials. These theoretical studies were mainly based on the binding energies of reaction intermediates, assuming that the reaction barriers were rather small [15]. To further understand the ORR, one may need to obtain quantitative information of reaction kinetics such as reaction barriers.

On the cathode in alkaline solutions, O₂ can be reduced over metal catalysts following two different mechanisms:

(i) Associative mechanism, which can be described as follows:

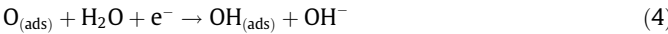


* Corresponding authors. Fax: +44 (0) 28 9097 6524 (P. Hu), +86 411 8437 9128 (X. Bao).

E-mail addresses: p.hu@qub.ac.uk (P. Hu), xhbaod@dicp.ac.cn (X. Bao).

¹ Fax: +86 411 8437 9128.

² Fax: +44 (0) 28 9097 6524.



where $*$ denotes a free site on the surface. Alternatively, instead of reaction (3), $\text{OOH}_{(\text{ads})}$ may desorb from the surface,



(ii) Dissociative mechanism, in which the first step is the following:



followed by steps (4) and (5).

Okamoto et al. simulated the ORR process on N-graphene surfaces in acid media using first-principles molecular dynamics [16]. They found that O_2 is reduced to H_2O through an associative mechanism analogous to that on Pt. Ozaki and co-workers studied the adsorption barriers of O_2 on different sites of N-doped graphene and found several structures that facilitate the adsorption of O_2 [17]. These pioneering studies provided preliminary understandings on N-graphene catalyzed ORR. However, detailed kinetics and thermodynamics of the whole reaction pathways of the two ORR mechanisms are still not clear, and the rate-determining step is unknown. Addressing these issues will give a clearer picture of the ORR mechanism and the origin of the catalytic activity of N-graphene.

The detailed kinetics and thermodynamics of the reaction system depend on many factors, such as the surface coverage, electrode potential, solvent effect, and pH. It is rather challenging to include very accurately these effects in simulations. We present the overall energy profile of ORR including the barrier of each element step by taking all these factors into account approximately in our calculations, aiming to acquire the basic chemistry of ORR on N-graphene. The paper is organized as follows. Following this Introduction section, the calculation details, including structural models, water effects, surface coverages, and transition state locating, are given in the Methods section. Then, Results and discussion are presented followed by the section of Conclusions.

2. Methods

2.1. DFT calculations

All the electronic structure calculations were performed using the Vienna Ab-initio Simulation Package (VASP) with the projector augmented wave method [20–26] and a cutoff energy of 400 eV [27]. The generalized gradient approximation method with PBE functional for the exchange-correlation term was used [28,29]. A $2 \times 2 \times 1$ Monkhorst-Pack \mathbf{k} -point sampling was used for the graphene unit cell of 6×6 [30]. For the unit cells of 12×12 ($29.544 \text{ \AA} \times 29.544 \text{ \AA}$), a $1 \times 1 \times 1$ Monkhorst-Pack \mathbf{k} -point sampling was utilized and testing results showed that the error of this \mathbf{k} -point sampling is negligible. The convergence of energy and forces were set to 1×10^{-4} eV and $0.03 \text{ eV}/\text{\AA}$, respectively.

2.2. Graphene models

Here we used a 6×6 supercell of graphene doped with six graphitic nitrogen atoms. Only graphitic N was considered for simplicity. This model gives a N concentration of 8.33%, close to the value in our previous experimental N-graphene sample, which exhibits good performance in catalytic ORR [11]. To study the dependence of reaction kinetics on N-doping configurations, two models with N distributed in different ways were used. In structure one (S1), the N atoms were mainly separated by two C atoms, while in structure two (S2), the N atoms were mainly separated by three C

atoms, as shown in Fig. 1. The specific sites of N were randomly set according to these rules. The supercells were in a hexagonal lattice with the unit cell vectors a and b in the surface plane and c vertical to the graphene plane. a and b were set as those of optimized graphene from DFT calculations ($a = b = 14.772 \text{ \AA}$ for 6×6) and c was set to 13 \AA which should be large enough to avoid interplanar interactions.

2.3. Water effect on the stabilities of intermediates

Since reactions occur in the presence of water in alkaline fuel cells, the effects of water may directly affect the stability of intermediates and the reaction barriers because all intermediates in both mechanisms ($\text{O}_{2(\text{ads})}$, $\text{OOH}_{(\text{ads})}$, $\text{OH}_{(\text{ads})}$, and $\text{O}_{(\text{ads})}$) are oxygen-containing species, which may form hydrogen bonding with H_2O molecules. Therefore, the effects may not be negligible.

In this work, the change on the formation free energy of intermediates due to the water effect was calculated as the stabilization energy. Several water layers consisting 41 H_2O molecules in the supercell with a density of 1 g/cm^3 were utilized to simulate the water environment, as shown in Fig. 2. The surface that is already occupied by one $\text{O}_{(\text{ads})}$ was used to simulate the water effect under the condition close to the real process. The initial structure of water layers was set as that of ice. To obtain the stable state of water layers, we ran molecular dynamics (MD) calculations to relax the water molecules until the total energy of the system was stabilized (~25 picoseconds). In the MD simulations, graphene and adsorbed intermediates were fixed. Then for each intermediate, at least six structures from MD simulations were chosen to be optimized and the most stable one was used to calculate the effect of water on the formation energy of intermediate in comparison with the system without water. In the subsequent calculations, the stabilization energy of each intermediate owing to water effect was used as a correction on the reaction energy in the absence of water molecules.

2.4. Surface coverages

In the previous experimental study [11], the cathode works under the condition of an onset potential of $\sim 0.04 \text{ V}$ (vs. NHE) and 1 M KOH solution saturated with O_2 (1 atm) at 298 K. Under this condition, the following reactions should occur:



It is expected, therefore, that under the steady state condition, the graphene surface is covered with a certain amount of the intermediates of reactions (8) and (9) ($\text{O}_{(\text{ads})}$ and $\text{OH}_{(\text{ads})}$) which are in quasi-equilibrium with liquid H_2O .

We obtained the surface coverages of $\text{O}_{(\text{ads})}$ and $\text{OH}_{(\text{ads})}$ by calculating the surface equilibrium state with H_2O using the thermodynamic method in Ref [15]. The surface equilibrium state was determined by increasing the coverages of $\text{O}_{(\text{ads})}$ and $\text{OH}_{(\text{ads})}$ on the graphene surfaces until the differential reaction free energy satisfies $\Delta G = 0$. At 298 K with the electropotential 0 V and $\text{pH} = 0$, the reaction $1/2\text{H}_2$ (1 atm) $\rightarrow \text{H}^+ + \text{e}^-$ is in equilibrium. Hence, by referring the potential to that of the normal hydrogen electrode, we can use the free energy of $1/2\text{H}_2$ (1 atm) instead of that of H^+ (1 M) $+ \text{e}^-$, upon which the free energy of H^+ (10^{-14} M) $+ \text{e}^-$ can be obtained by adding a correction energy in pH : $\Delta G(\text{pH}) = kT \ln[\text{H}^+] = -\text{pH} \cdot kT \ln 10$, where $\text{pH} = 14$. The effect of a bias was included for all the states that involve electron transfer in the reactions by adding a shift on the free energy: $\Delta G(U) = n\text{eU}$, where n is number of electrons transferred and U is

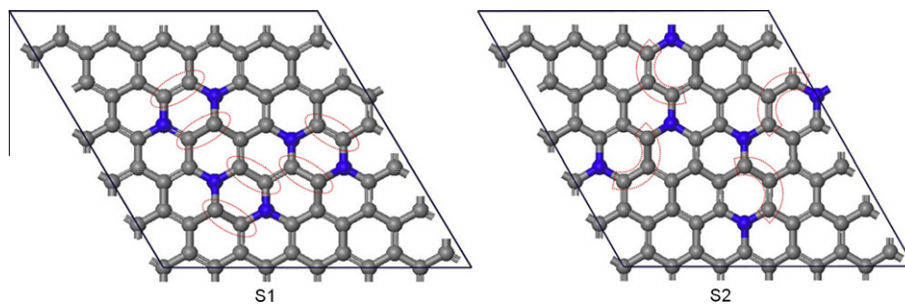


Fig. 1. Illustration of nitrogen distributions in two 6×6 supercells. In structure one (S1), the N atoms are separated by two C atoms while in structure two (S2) the N atoms are separated by three C atoms. Thus, S1 possesses a more concentrated N distribution than that in S2. The gray and blue spheres represent C and N atoms, respectively.

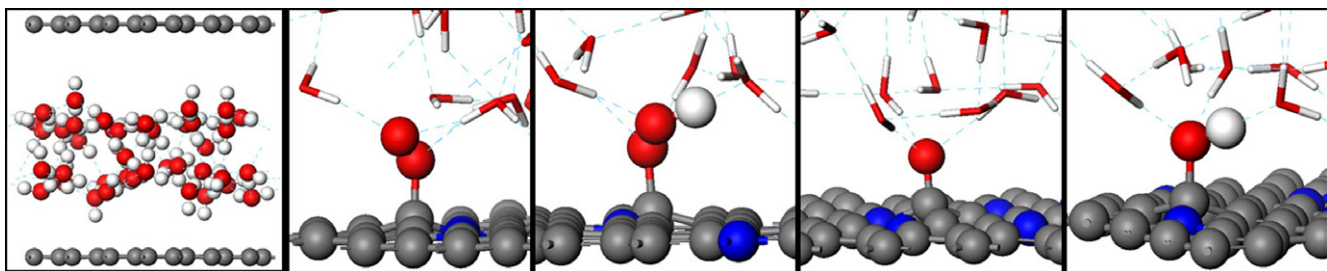


Fig. 2. Structures of water layers. From the left: water layers on the clean surface, the surfaces with adsorbed O_2 , OOH , O , and OH , respectively. The gray, blue, red, and white spheres represent C, N, O, and H atoms, respectively. (For interpretation of the references to color in this figure legend, the reader is referred to the web version of this article.)

the electrode potential. In our calculations, we used $U = 0.04$ V (vs. NHE). This approach of considering the bias effect has been proved efficient without much loss of accuracy in electrochemical reactions [31,32]. In the electrochemical reactions, the adsorbed species also interact with the electric field due to the electrochemical double layer which can be simplified into the coupling interaction between the dipole moments of adsorbed species and the electric field [33–35]. However, this effect has been proved subtle for the intermediates in ORR and does not affect the results much [36]. Thus, although it was partially considered in approach (iv) (see section 2.5), we will to a large extent neglect this in our calculations.

The free energies of the intermediates were obtained by $G = E_{\text{total}} + ZPE - TS$, where E_{total} is the total energy of species, ZPE is the zero point energy, and S is the entropy. The free energy of H_2O in bulk water was calculated in the gas phase with a pressure of 0.035 bar, which is the equilibrium vapor pressure of H_2O at 298 K. The free energy of O_2 was derived as $G(O_2) = 2G(H_2O) - 2G(H_2) - 4.92$ eV from the free energy change of the reaction $O_2 + 2H_2 \rightarrow 2H_2O$ which is 4.92 eV under the standard condition. The free energy of OH^- was derived as $G(OH^-) = G(H_2O) - G(H^+)$ because the reaction $H^+ + OH^- \rightarrow H_2O$ is in equilibrium in water solution. In this study, the entropies of molecules in the gas phase were obtained from the literature [37].

2.5. Transition states (TSs)

The TS of each elementary reaction was searched using the constrained minimization approach [38–40] in the presence of water molecules according to the following procedure: (i) several layers of water with the density of 1 g/cm^3 were placed above the surface and then MD calculations were carried out for ~ 25 ps; (ii) at least six structures selected from MD calculations were optimized and the most stable structure was obtained; and (iii) the TS was searched in the most stable structure. In electrochemical systems, reactions occur usually on charged electrodes. To obtain the accurate TSs, it may be essential to consider the charges, as well as the

double layer, which can also affect reaction barriers. Several groups have explored methods to calculate charged electrode systems. Taylor et al. [42] and Filhol and Neurock [41] developed similar methods to determine the charges in the system by tuning the work function Φ of the system according to the electrode potential U via adding or subtracting electrons from the slab. Nørskov and coworkers [43,44] and Taylor et al. [42] also proposed to add H or alkaline metal atoms into the system to tune the Φ of the surface according to U (Eq. (10)). Therefore, we used four different approaches based on the methods proposed above to calculate the TSs on electrodes.

In approach (i), all the TSs were calculated in the presence of water with no charge in the systems using 6×6 supercells.

In approach (ii), we first located the TS of each reaction step on the N-graphene without charge using 6×6 supercells. Φ of each TS was calculated and adjusted to the correct value according to U (Eq. (10)) by adding electrons into the system. Then, each TS was refined in the charged system. The change of Φ due to this refinement was neglected because of the very small structure change. The initial state (IS) of each reaction step was determined with the same charge as that of the corresponding TS.

During reaction, all the intermediates may exist simultaneously on the catalyst surface but in different coverages. Usually, one species may dominate over others with a larger population and the surface work function may be significantly affected by this species. In approach (iii), we used a larger surface (12×12 supercell) that is occupied by dominant species to calculate TSs. The dominant species was derived from the rate-determining step determined from approach (i), which is in fact the same from all approaches in this work (see Section 3.3.2). Then, Φ of the surface was adjusted to the correct value according to U by adding electrons. Finally, the TS of each step was located on the surface with the fixed number of electrons.

In approaches (ii) and (iii), a compensating background charge was distributed homogeneously over the unit cell to maintain overall charge neutrality which is a common approach implemented in VASP.

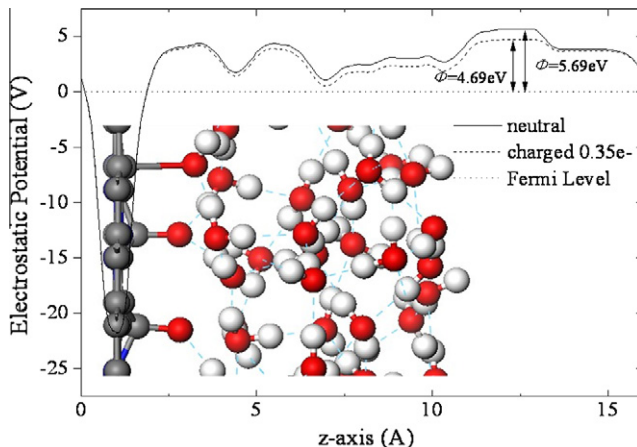


Fig. 3. The electrostatic potential profile averaged on the surface plane as a function of the z-axis of the supercell in the transition state of $\text{OH}_{(\text{ads})}$ desorption on S1 in approach (ii) (see Section 2.5). The work function of the neutral system is 5.69 eV. After adding 0.35 electrons, the work function is decreased to the experimental value (4.69 eV). In the vacuum region, a dipole correction is introduced in the calculation in order to electrostatically decouple the periodically repeated slabs in the z-direction.

In approach (iv), the procedure was the same as that in approach (iii) except that instead of adding electrons to the system to adjust Φ , potassium atoms were used to establish an outer Helmholtz plane. K atoms are anticipated to ionize, thus transferring their electrons to the N-graphene surface. This approach establishes a more naturally derived potential and also an approximated double layer. This method is restrictive in that only an integral number of K atoms can be added to the unit cell. Since the unit cell in this model is rather large (12×12) so that Φ changes in small steps as K atoms were added into the system, Φ can still be tuned to the correct value with neglectable errors (~ 0.05 eV).

In approaches (ii), (iii), and (iv), the electrode potential U was obtained by referring the work function Φ of the system to the absolute potential of NHE (U_{NHE}) via the following equation

$$U = 0.04V = \Phi/e - U_{\text{NHE}} \quad (10)$$

where 0.04 V is the experimental onset potential. The value of U_{NHE} has been reported in the range from 4.44 to 4.85 V [45–48]. Our calculations show that an uncertainty of ~ 0.20 V on the electropotential causes an error of ~ 0.03 eV on the reaction barrier. Therefore, we used 4.65 V for U_{NHE} , expecting no significant effect on our results. In approaches (ii) and (iii), the work function Φ was calculated by adding a thin (~ 3 Å) vacuum layer above the water layers, as proposed by Filhol and Neurock [41]. In approach (iv), a ~ 7 -Å thick vacuum layer was set above the water layers. Tuning Φ of the TS for $\text{OH}_{(\text{ads})}$ desorption on S1 following approach (ii) is shown in Fig. 3 as an example.

3. Results and discussion

3.1. Water effect on the stabilities of intermediates

As mentioned before, the interaction between water molecules and intermediates may significantly affect the stability of the surface species on N-graphene. Therefore, we first studied the water effect. This effect can vary depending on the number of hydrogen bonds between the water molecules and the intermediates in the system. Since the local distribution of the intermediates may affect the formation of hydrogen bonds, the N-graphene S1 that is already bonded with one $\text{O}_{(\text{ads})}$ was used to simulate the local

Table 1

The free energy changes of adsorption of O_2 , O , OH , and OOH with (ΔG_{water}) and without (ΔG) water on S1. The stabilization energies are obtained from $\Delta G_{\text{water}} - \Delta G$, which is a quantitative measure of water effect on the stability of the adsorbed species.

Species	$\text{O}_{2(\text{ads})}$	$\text{O}_{(\text{ads})}$	$\text{OH}_{(\text{ads})}$	$\text{OOH}_{(\text{ads})}$
ΔG (eV)	0.07	-0.43	0.02	-0.04
ΔG_{water} (eV)	-0.76	-0.96	-0.40	-0.53
Stabilization energy (eV)	-0.83	-0.53	-0.42	-0.49

surface condition and investigate the water effect for each species. A further increase of pre-adsorbed $\text{O}_{(\text{ads})}$ was found to exert only marginal (~ 0.05 eV) effect.

We first obtained the free energy change (ΔG) of the formation of each species without water as a reference, which are listed in Table 1. Then, in the presence of water molecules, the free energy change (ΔG_{water}) was calculated (Table 1). The stabilization energy was defined as the difference between ΔG_{water} and ΔG . The data in Table 1 show that via hydrogen bonding water molecules can substantially stabilize the surface species. In particular, the stabilization energy of $\text{O}_{2(\text{ads})}$ is considerably large. In the absence of water molecules, O_2 cannot even adsorb on the N-graphene surface with the optimized distance from the surface to the nearest O atom of O_2 being ~ 2.87 Å. In contrast, in the presence of water molecules, the distance decreases to 1.47 Å and the chemisorption energy becomes -0.76 eV. This enhanced adsorption may be partially due to the polarization of O_2 molecule induced by hydrogen bonding. The Bader charge analysis [49–51] shows that O_2 possesses more negative charges (1.16 e $^-$) when surrounded by H_2O molecules than that without water (0.80 e $^-$), which indicates stronger interaction between O_2 and the N-graphene. Thus, the $\text{O}_{2(\text{ads})}$ stabilization energy of -0.83 eV may contain two parts, the hydrogen bonding energy and the enhanced adsorption energy. The stabilization energies were used in further calculations for surface coverages and reaction kinetics.

3.2. Surface coverages under reaction conditions

Previous work showed that the active sites of N-graphene for ORR were the carbon atoms adjacent to N [18,19]. In the 6×6 supercell which contains six nitrogen atoms, there are 18 carbon sites that may be the reaction centers. Therefore, we used $n/18$ to calculate the coverage, where n is the number of adsorbed species. At the potential of 0.04 V and pH of 14, we calculated the differential free energy change as a function of coverage for species of $\text{OH}_{(\text{ads})}$ and $\text{O}_{(\text{ads})}$, as shown in Fig. 4a. The energy values are listed in Table 2. The adsorption sites are illustrated in Fig. 4b and c.

It can be seen that in the exothermic region (below 1/6 ML), $\text{O}_{(\text{ads})}$ is always more stable than $\text{OH}_{(\text{ads})}$, which indicates that $\text{O}_{(\text{ads})}$ is the dominant species on the N-graphene surface. From zero to 1/9 ML, the formations of $\text{O}_{(\text{ads})}$ and $\text{OH}_{(\text{ads})}$ are both exothermic. As the coverage further increases to 1/6 ML, the formation energy is 0.28 eV endothermic for $\text{OH}_{(\text{ads})}$ but still -0.08 eV (exothermic) for $\text{O}_{(\text{ads})}$ on S1 whereas it is 0.00 eV for both species on S2. When the coverage increases further to 2/9 ML, however, the formation of both species is substantially endothermic on both surfaces. Therefore, it is clear that both S1 and S2 covered with 1/6 ML $\text{O}_{(\text{ads})}$ are in equilibrium with H_2O , suggesting that 1/6 ML $\text{O}_{(\text{ads})}$ is likely the surface coverage under reaction conditions. This strong coverage-dependent formation energy is mainly due to the high electronegativity of the surface species which results in substantial electron transfer from the surfaces to the species, as can be seen from the charge analysis of $\text{O}_{2(\text{ads})}$ species in Section 3.1.

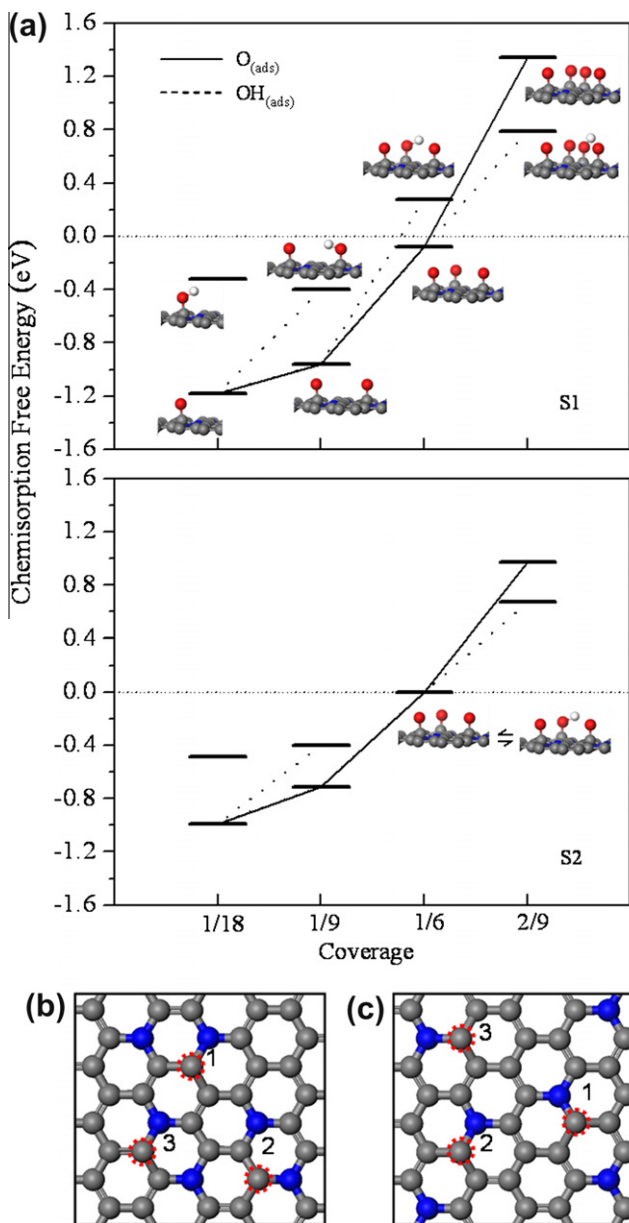


Fig. 4. (a) Differential chemisorption free energy profile of $O_{(ads)}$ and $OH_{(ads)}$ as a function of coverage. On S2 at coverage of 1/6 ML, the chemisorption energy of $OH_{(ads)}$ is the same as $O_{(ads)}$. (b) and (c) The adsorption sites on S1 and S2, respectively. The sites marked with red circles and denoted with numbers correspond to the adsorption sequence when the coverage is increased from 1/18 to 1/6 ML. The gray, blue, red, and white spheres represent C, N, O, and H atoms, respectively. (For interpretation of the references to color in this figure legend, the reader is referred to the web version of this article.)

Table 2

The differential free energy changes for the formation of $O_{(ads)}$ ($H_2O + * \rightarrow O_{(ads)} + 2H^+ + 2e^-$) and $OH_{(ads)}$ ($H_2O + * \rightarrow OH_{(ads)} + H^+ + e^-$) on S1 and S2 (Fig. 1) as a function of coverage. The stabilization energies from water effect are included.

Coverage	1/18	1/9	1/6	2/9
$\Delta G(O_{(ads)})$, (eV)	S1	-1.18	-0.96	-0.08
	S2	-0.99	-0.71	0.00
$\Delta G(OH_{(ads)})$, (eV)	S1	-0.32	-0.40	0.28
	S2	-0.49	-0.40	0.00
			0.79	0.79
			0.67	0.67

3.3. ORR kinetics

3.3.1. Reaction barriers

It remains a big challenge to calculate the reaction barriers in fuel cell systems due to three factors that should be taken into consideration: (i) reactions occur in liquid phase; (ii) catalyst surfaces possess some charges; and (iii) the electric double layers on the electrode surface may also affect reaction barriers. To the best of our knowledge, a full free energy profile with the barriers of all elementary steps has not been reported yet.

We used four approaches described in Section 2.5 to calculate the barriers. We first obtained the barriers on both S1 and S2 in the presence of water molecules in neutral system (approach (i)) as a reference. As analyzed in Section 3.2, 1/6 ML of $O_{(ads)}$ is likely the surface coverage under reaction conditions, it was chosen for reaction barrier calculations. If O_2 adsorption is considered as the “first” step of ORR, then there is no additional active site for O_2 adsorption at 1/6 ML $O_{(ads)}$ because all the three sites have been occupied by $O_{(ads)}$. Therefore, we removed the $O_{(ads)}$ on the third site to make a vacancy (site 3 in Fig. 4b and c) for O_2 adsorption. Alternatively, we removed the $O_{(ads)}$ via the hydrogenation and thus this became the “first” step of ORR. Because the reaction is a catalytic cycle, both approaches will yield exactly the same kinetic result. The calculated barriers (E_{a1}) are listed in Table 3.

Then we calculated TSs on charged surfaces with the approaches (ii–iv) described in Section 2.5 and the results are shown in Table 3. In approach (ii) with the 6×6 supercells, the work function of different TS systems was tuned via adding various amounts of electrons (Fig. 5). In approach (iii) with 12×12 supercell of S1, for all the TSs a fixed number of electrons were added to tune the work function to 4.69 eV. From Table 3, we can see that on S1 the results from the approaches (ii) and (iii) are close to each other, also to the results of approach (iv) which simulates more naturally charged surfaces. We can also see that the reaction barriers are considerably affected by the electropotential. This can be understood as follows: These elementary steps involve significant electrons transfer; this leads to the change of the work function of the surface which may affect the stabilization of the TSs. Therefore, it is important to take this effect into account in the barrier calculations if quantitative results are needed. However, all the approaches give similar general trends in the system. Therefore, it is likely that the same chemistry will be obtained from any of these approaches.

3.3.2. Reaction mechanisms

Since the four approaches give similar chemistry, we used the energies from the second approach (E_{a2}) to discuss the reaction mechanism. Possible reaction pathways are illustrated in Scheme 1.

The free energy profiles are shown in Fig. 6a. Let us first concentrate on S1. The first step is the adsorption of O_2 on site 3 followed by two paths; $O_{2(ads)}$ can accept a proton from H_2O to form $OOH_{(ads)}$ or directly dissociate to yield two $O_{(ads)}$, i.e., the

Table 3

The reaction barriers on both S1 and S2. E_{a1} , E_{a2} , E_{a3} , and E_{a4} are the barriers using the approaches (i), (ii), (iii), and (iv), respectively. $O_2 \cdot \cdot H$ is the reaction of proton transfer to $O_{2(ads)}$ from H_2O ; $O \cdot \cdot OH$ is the breakage of O–O bond of $OOH_{(ads)}$; $O \cdot \cdot H$ is the reaction of a proton transfer to $O_{(ads)}$ from H_2O ; $C \cdot \cdot OH$ is the reaction of $OH_{(ads)}$ removal.

TS	$O_2 \cdot \cdot H$	$O \cdot \cdot OH$	$O \cdot \cdot H$	$C \cdot \cdot OH$
S1	E_{a1}	0.61	0.72	0.88
	E_{a2}	0.42	0.56	0.54
	E_{a3}	0.43	0.46	0.57
	E_{a4}	–	–	0.44
S2	E_{a1}	0.45	0.57	0.81
	E_{a2}	0.35	0.27	0.36

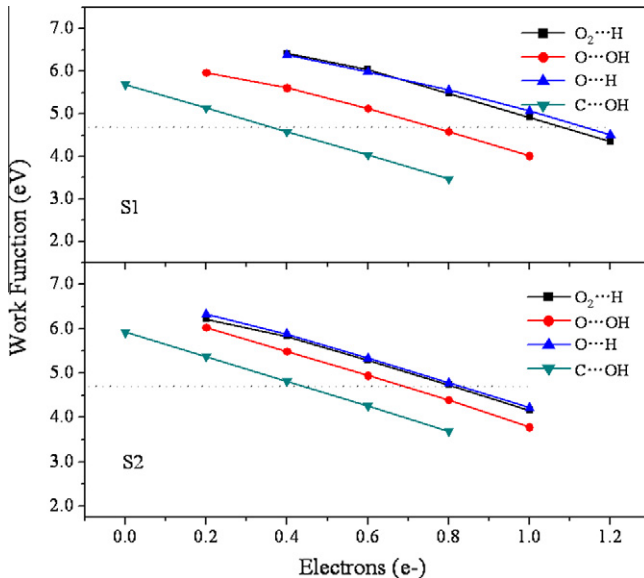


Fig. 5. Work functions of the transition states as a function of the number of electrons added into the systems. The dot line denotes the experimental work function of cathode (4.69 eV). $O_2 \cdots H$ represents the transition state of proton transfer to $O_{2(\text{ads})}$ from H_2O ; $O \cdots OH$ indicates the O–O bond breaking of $OOH_{(\text{ads})}$; $O \cdots H$ denotes the transfer of proton to $O_{(\text{ads})}$ from H_2O ; $C \cdots OH$ denotes the removal of $OH_{(\text{ads})}$.

associative or dissociative mechanisms, respectively. The dissociation barrier of $O_{2(\text{ads})}$ in the presence of water is 1.56 eV which is remarkably higher than that of the associative reduction step to form $OOH_{(\text{ads})}$ with an effective barrier of 0.51 eV, as can be seen from Fig. 6a. A similar result is obtained on S2. It is clear that at the working temperature of alkaline fuel cell (~ 350 K), the barrier of 1.56 eV is too high for $O_{2(\text{ads})}$ dissociation to occur with a reasonable rate on the N-graphene surface. Therefore, the more energetically favored associative mechanism should be dominating in the reduction of O_2 .

The barrier of the $O_{2(\text{ads})}$ hydrogenation to form $OOH_{(\text{ads})}$ is 0.42 eV from approach (ii) and 0.43 eV from approach (iii), which is slightly higher than that reported previously on Pt(1 1 1) (~ 0.3 eV) in the presence of water [52], but still moderate for low temperature reactions. Following hydrogenation, $OOH_{(\text{ads})}$ may desorb from the surface to give OOH^- , or alternatively the O–O bond of $OOH_{(\text{ads})}$ may break to yield $O_{(\text{ads})}$ and OH^- . Our calculation shows that the $OOH_{(\text{ads})}$ desorption is energetically unfavorable with an energy loss of 0.22 eV (endothermic), as illustrated in Fig. 6a. In contrast, the O–O bond scission is strongly exothermic with an overall barrier of 0.56 eV from approach (ii) and 0.46 eV from approach (iii). This is in agreement with experimental results that only traces of peroxide are produced [10]. In the subsequent step, the barrier of hydrogenation of $O_{(\text{ads})}$ was calculated to be almost the same (~ 0.55 eV) from all the approaches

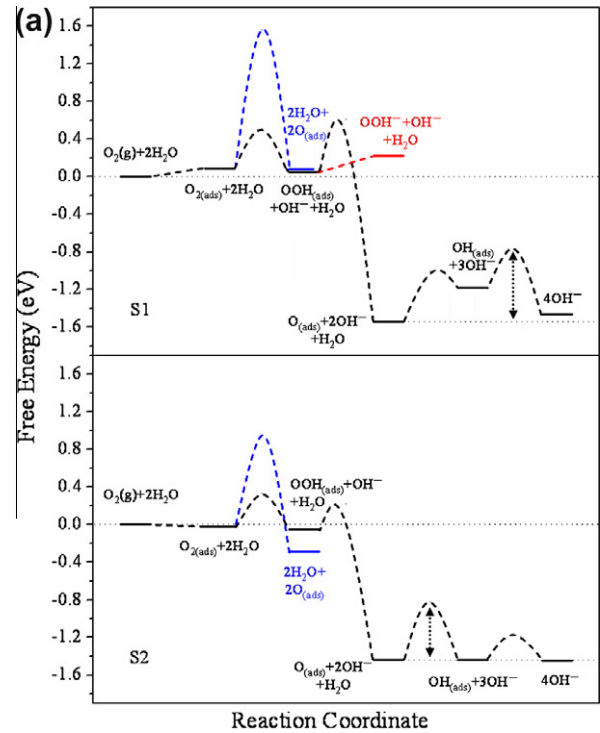
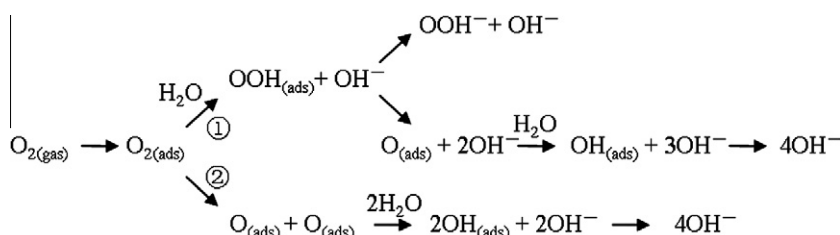


Fig. 6. (a) Free energy diagram for O_2 reduction on S1 and S2 under the condition of 0.04 V and pH = 14. The black line indicates the intermediates and reaction barriers of associative mechanism. The blue line indicates the dissociative barrier of O_2 and the intermediate. The red line indicates the formation of OOH^- . (b) Intermediate structures of associative mechanism on S1 and S2. From the left to right: $O_{2(\text{ads})}$, $OOH_{(\text{ads})}$, $O_{(\text{ads})}$, and $OH_{(\text{ads})}$. The gray, blue, red, and white spheres represent C, N, O, and H atoms, respectively. (For interpretation of the references to color in this figure legend, the reader is referred to the web version of this article.)

except approach (i). In the last step, the removal of $OH_{(\text{ads})}$ needs to overcome a barrier of 0.42 eV, giving rise to the overall barrier of 0.78 eV to remove $O_{(\text{ads})}$. Using the kinetic analysis model proposed by Kozuch and Shaik [53,54] in our system, we found that the step of the removal of $O_{(\text{ads})}$ is the rate-determining step. This is similar to previous theoretical results on Pt(1 1 1), where the rate of OH removal determined the overall ORR activity [55,56].



Scheme 1. Reaction scheme of ORR on N-graphene in alkaline solution, where ① presents an associative mechanism and ② a dissociative mechanism.

3.3.3. Structural effects

Comparing the two energy profiles on S1 and S2 using approach (ii) (Fig. 6a), we can see similarities regarding the reaction mechanisms. The dissociation barriers of O₂ on these two surfaces are too high and the associative mechanism is favored. In the associative mechanism, the removal of O_(ads) exhibits the highest barrier. Therefore, ORR on N-graphene surfaces likely follows the associative mechanism in alkaline solution and the reaction rate is limited by the O_(ads) removal from the surface.

However, one also sees that the two energy profiles have their own characteristics. The overall barrier of the first reduction step (O_{2(ads)} + H₂O → OOH_(ads) + OH⁻) on S2 (0.33 eV) is lower than that on S1 (0.51 eV). In the subsequent step, the O–O bond (OOH_(ads) → O_(ads) + OH⁻) is more difficult to break on S1 than that on S2 with the overall barriers of 0.61 eV and 0.22 eV, respectively. In the last step, the removal of OH_(ads) on S2 also possesses a smaller barrier (0.32 eV) than that on S1 (0.42 eV). The hydrogenation of O_(ads) (O_(ads) + H₂O → OH_(ads) + OH⁻) is the only step where on S2 it gives a slightly higher barrier (0.62 eV) than that on S1 (0.54 eV). However, the last two steps (O_(ads) + H₂O → OH_(ads) + OH⁻ → 2OH⁻) can be combined to form an effective step of O_(ads) desorption (O_(ads) + H₂O → 2OH⁻) and its overall barrier is 0.78 eV on S1, larger than that on S2 (0.62 eV).

The above results suggest that S2 is more active than S1 for ORR. This activity difference can be understood from the formation energies of O_(ads). As shown in Fig. 4a and Table 2, the formation energies of O_(ads) on S1 are always lower (more exothermic) than those on S2. A stronger intermediate-surface bonding usually leads to a higher association barrier for the subsequent reaction of intermediates, as demonstrated in CO oxidation by Liu and Hu [57]. The different formation energies of O_(ads) on the two structures are attributed to their distinct local N distributions. On S1, the local concentration of nitrogen atoms is higher than that on S2 (Fig. 1). The effect of local N concentration on activity will be investigated in a further study.

4. Conclusion

By taking into account the experimental conditions, i.e., the surface coverage, the water effect, the bias effect, and pH, this work presents a systematic theoretical study on the full reaction path of ORR on graphitic-N-doped graphene surfaces. A deeper understanding of the ORR activity of N-graphene is obtained. The key findings are summarized as follows:

- (i) The water effect is essential in constructing a reliable reaction free energy profile, especially for O₂ adsorption which is significantly enhanced by the polarization of O₂ due to hydrogen bonding with H₂O. Without water, O₂ cannot even adsorb on the N-graphene surface.
- (ii) The dissociation barrier of O₂ is too high for the reaction to achieve a reasonable rate, whereas the more energetically favored associative mechanism is dominating for ORR.
- (iii) The desorption of OOH_(ads) to form OOH⁻ is found to be energetically unfavored compared with the reaction OOH_(ads) → O_(ads) + OH⁻, which suggests that O₂ is mainly reduced via a “4e⁻ reduction” pathway on N-doped graphene.
- (iv) Four approaches were used for locating the transition states on charged surfaces, which lead to similar chemistry in ORR kinetics. The rate-determining step is the removal of O_(ads) from the N-graphene surface. Thus, a more active catalyst should possess a structure which can further facilitate the desorption of O_(ads) species.

Acknowledgment

We gratefully acknowledge the financial support from the Natural Science Foundation of China (Grant Nos. 11079005 and 21033009).

Appendix A. Supplementary material

Supplementary data associated with this article can be found, in the online version, at doi:10.1016/j.jcat.2011.06.015.

References

- [1] S. Maldonado, K.J. Stevenson, J. Phys. Chem. B 109 (2005) 4707.
- [2] J. Ozaki, N. Kimura, T. Anahara, A. Oya, Carbon 45 (2007) 1847.
- [3] J. Ozaki, T. Anahara, N. Kimura, A. Oya, Carbon 44 (2006) 3358.
- [4] Y. Shao, J. Sui, G. Yin, Y. Gao, Appl. Catal. B 79 (2008) 89.
- [5] P.H. Matter, U.S. Ozkan, Catal. Lett. 109 (2006) 115.
- [6] N.P. Subramanian, X. Li, V. Nallathambi, S.P. Kumaraguru, H. Colon-Mercado, G. Wu, J.-W. Lee, B.N. Popov, J. Power Sources 188 (2009) 38.
- [7] H. Niwa, K. Horiba, Y. Harada, M. Oshima, T. Ikeda, K. Terakura, J. Ozaki, S. Miyata, J. Power Sources 187 (2009) 93.
- [8] K.R. Lee, K.U. Lee, J.W. Lee, B.T. Ahn, S.I. Woo, Electrochim. Commun. doi:10.1016/j.jelecom.2010.05.023.
- [9] K. Gong, F. Du, Z. Xia, M. Durstock, L. Dai, Science 323 (2009) 760.
- [10] L. Qu, Y. Liu, J.B. Baek, L. Dai, ACS Nano. 4 (2010) 1321.
- [11] D.H. Deng, X.L. Pan, L. Yu, Y. Cui, Y.P. Jiang, J. Qi, W.X. Li, Q. Fu, X.C. Ma, Q.K. Xue, G.Q. Sun, X.H. Bao, Chem. Mater. 23 (2011) 1188.
- [12] B.N. Grgur, N.M. Marković, P.N. Ross, Can. J. Chem. 75 (1997) 1465.
- [13] J. Rossmeisl, A. Loggottir, J.K. Nørskov, Chem. Phys. 319 (2005) 178.
- [14] J. Rossmeisl, Z.W. Qu, H. Zhu, G.J. Kroes, J.K. Nørskov, J. Electroanal. Chem. 607 (2007) 83.
- [15] J.K. Nørskov, J. Rossmeisl, A. Loggottir, L. Lindqvist, J.R. Kitchin, T. Bligaard, H. Jónsson, J. Phys. Chem. B 108 (2004) 17886.
- [16] Y. Okamoto, Appl. Surf. Sci. 256 (2009).
- [17] T. Ikeda, M. Boero, S.F. Huang, K. Terakura, M. Oshima, J. Ozaki, J. Phys. Chem. C 112 (2008) 14706.
- [18] S.F. Huang, K. Terakura, T. Ozaki, T. Ikeda, M. Boero, M. Oshima, J. Ozaki, S. Miyata, Phys. Rev. B 80 (2009) 235410.
- [19] S.S. Yu, W.T. Zheng, Q.B. Wen, Q. Jiang, Carbon 46 (2008) 537.
- [20] G. Kresse, J. Hafner, Phys. Rev. B 48 (1993) 13115.
- [21] G. Kresse, J. Furthmüller, Phys. Rev. B 54 (1996) 11169.
- [22] G. Kresse, J. Hafner, Phys. Rev. B 47 (1993) 558.
- [23] G. Kresse, J. Hafner, Phys. Rev. B 49 (1994) 14251.
- [24] G. Kresse, J. Furthmüller, Comput. Mater. Sci. 6 (1996) 15.
- [25] P.E. Blochl, Phys. Rev. B 50 (1994) 17953.
- [26] G. Kresse, D. Joubert, Phys. Rev. B 59 (1999) 1758.
- [27] We checked the energy convergence with respect to the cutoff energy by using 450 eV and 500 eV for the chemisorption free energy of O_(ads) on graphene structure 1 (S1) at the coverage of 1/18 ML (the data of Table 2 in the manuscript). It was found that ΔG(O_(ads)) is -1.17 eV and -1.19 eV for 450 eV and 500 eV cutoff-energies, respectively, which is very close to -1.18 eV from 400 eV cutoff-energy.
- [28] J.P. Perdew, K. Burke, M. Ernzerhof, Phys. Rev. Lett. 77 (1996) 3865.
- [29] J.P. Perdew, K. Burke, M. Ernzerhof, Phys. Rev. Lett. 78 (1997) 1396.
- [30] H.J. Monkhorst, J.D. Pack, Phys. Rev. B 13 (1976) 5188.
- [31] J. Rossmeisl, J.K. Nørskov, C.D. Taylor, M.J. Janik, M. Neurock, J. Phys. Chem. B 110 (2006) 21833.
- [32] Y.H. Fang, Z.P. Liu, J. Phys. Chem. C 113 (2009) 9765.
- [33] M.P. Hyman, J.W. Medlin, J. Phys. Chem. B 109 (2005) 6304.
- [34] M.P. Hyman, J.W. Medlin, J. Phys. Chem. B 110 (2006) 15338.
- [35] S.A. Wasileski, M.T.M. Koper, M.J. Weaver, J. Am. Chem. Soc. 124 (2002) 2796.
- [36] G.S. Karlberg, J. Rossmeisl, J.K. Nørskov, Phys. Chem. Chem. Phys. 9 (2007) 5158.
- [37] <http://cccbdb.nist.gov/>.
- [38] A. Alavi, P. Hu, T. Deutsch, P.L. Silvestrelli, J. Hutter, Phys. Rev. Lett. 80 (1998) 3650.
- [39] A. Michaelides, P. Hu, J. Am. Chem. Soc. 122 (2000) 9866.
- [40] Z.-P. Liu, P. Hu, J. Am. Chem. Soc. 125 (2003) 1958.
- [41] J.S. Filhol, M. Neurock, Angew. Chem. Int. Ed. 45 (2006) 402.
- [42] C.D. Taylor, S.A. Wasileski, J.S. Filhol, M. Neurock, Phys. Rev. B 73 (2006) 165402.
- [43] E. Skúlason, G.S. Karlberg, J. Rossmeisl, T. Bligaard, J. Greeley, H. Jónsson, J.K. Nørskov, Phys. Chem. Chem. Phys. 9 (2007) 3241.
- [44] J. Rossmeisl, E. Skúlason, M.E. Björketun, V. Tripkovic, J.K. Nørskov, Chem. Phys. Lett. 466 (2008) 68.
- [45] J.O.M. Bockris, S.D. Argade, J. Chem. Phys. 49 (1968) 5133.
- [46] R. Gomer, G. Tryson, J. Chem. Phys. 66 (1977) 4413.
- [47] H. Reiss, A. Heller, J. Phys. Chem. 89 (1985) 4207.
- [48] D. Tsiplikides, C.G. Vayenas, Solid State Ionics 152–153 (2002) 625.

- [49] W. Tang, E. Sanville, G. Henkelman, *J. Phys.: Condens. Matter* 21 (2009) 084204.
- [50] E. Sanville, S.D. Kenny, R. Smith, G. Henkelman, *J. Comput. Chem.* 28 (2007) 899.
- [51] G. Henkelman, A. Arnaldsson, H. Jónsson, *Comput. Mater. Sci.* 36 (2006) 254.
- [52] M.J. Janik, C.D. Taylor, M. Neurock, *J. Electrochem. Soc.* 156 (2009) B126.
- [53] S. Kozuch, S. Shaik, *J. Phys. Chem. A* 112 (2008) 6032.
- [54] S. Kozuch, S. Shaik, *Acc. Chem. Res.* (2010). doi:10.1021/ar1000956.
- [55] V. Tripkovic, E. Skúason, S. Siahrostami, J.K. Nørskov, J. Rossmeisl, *Electrochim. Acta* (2010). doi:10.1016/j.electacta.2010.02.056.
- [56] A.U. Nilekar, M. Mavrikakis, *Surf. Sci.* 602 (2008) L89.
- [57] Z.-P. Liu, P. Hu, *J. Chem. Phys.* 115 (2001) 4977.